

Stabilizing impact of high gradient of β on microturbulence

C. Bourdelle^{a)}

Association Euratom-CEA, CEA/DSM/DRFC, CEA Cadarache, 13108 Saint-Paul-lez-Durance, France

W. Dorland

Department of Physics, University of Maryland, College Park, Maryland 20742

X. Garbet

Association Euratom-CEA, CEA/DSM/DRFC, CEA Cadarache, 13108 Saint-Paul-lez-Durance, France

G. W. Hammett

Princeton Plasma Physics Laboratory, Princeton University, Princeton, New Jersey 08543

M. Kotschenreuther

Institute for Fusion Studies, University of Texas at Austin, Austin, Texas 78712

G. Rewoldt and E. J. Synakowski

Princeton Plasma Physics Laboratory, Princeton University, Princeton, New Jersey 08543

(Received 6 March 2003; accepted 30 April 2003)

It is shown here that microturbulence can be stabilized in the presence of steep temperature and density profiles. Indeed in high β plasmas, pressure profile gradients are associated with high $|\beta'| = -\partial\beta/\partial\rho$, where $\beta = P/(B^2/2\mu_0)$ and ρ the square root of the toroidal flux normalized to its edge value. It is shown here that high values of $|\beta'|$ have a stabilizing influence on drift modes. This may form the basis for a positive feedback loop in which high core beta values lead to improved confinement, and to further increase in β . A gyrokinetic electromagnetic flux tube code, GS2 [M. Kotschenreuther, G. Rewoldt, and W. M. Tang, *Comput. Phys. Commun.* **88**, 128 (1995)], is used for analyzing the microstability. In high β spherical tokamak plasmas, high $|\beta'|$ rather than low aspect ratio is a source of stabilization. Therefore, the effect of high $|\beta'|$ should be stabilizing in the plasmas of the National Spherical Torus Experiment [Y.-K. Peng, M. G. Bell, R. E. Bell *et al.*, *Phys. Plasmas* **7**, 1681 (2000)]. © 2003 American Institute of Physics. [DOI: 10.1063/1.1585032]

I. INTRODUCTION

In most tokamak plasmas, heat transport is mainly due to microturbulence. In order to achieve efficient fusion plasmas, it is of prime importance to reduce turbulent transport. Such reductions necessarily lead to steepened density and temperature profiles. With this as motivation, the stabilizing impact of $|\beta'|$ on microstability is studied here. Microstability analyses are performed using a gyrokinetic flux tube code, GS2 (Refs. 1 and 2), in its linear version. The initial value code, GS2, is benchmarked with the eigenvalue code FULL (Refs. 3 and 4) at high β . The analytically reconstructed Miller equilibrium as given in Ref. 5, valid for noncircular, finite aspect ratio magnetic surfaces as well as numerically computed magnetic equilibria are used. We show that the curvature and the ∇B drifts are strongly reduced by high $|\beta'|$. Once the ∇B and curvature drift direction is reversed by high $|\beta'|$, no drive remains for the dominant interchange instability. As shown in this paper, it is important to include the perturbations parallel to the magnetic field, δB_{\parallel} , in the microstability analysis of high β plasmas, as already pointed out in Refs. 6, 7 and recently in the context of spherical tokamak in Ref. 8. Neglecting this component of the fluctuating magnetic field leads to a severe underestimation of the instability growth rates. But even after including δB_{\parallel} , the stabilizing effect of high $|\beta'|$ can induce enhanced tempera-

ture and density peaking, leading to even higher values of $|\beta'|$. As suggested in the case of $\mathbf{E} \times \mathbf{B}$ shear stabilization, there is a possibility for entering a positive feedback loop with respect to turbulence suppression, β' , and enhanced confinement. Finally it is shown that in high β National Spherical Torus Experiment (NSTX) plasmas, high $|\beta'|$ rather than low aspect ratio is believed to be responsible for lower growth rates than in a tokamak case at higher aspect ratio and lower β . Therefore, high β NSTX plasmas are ideally suited for the study of a possible route to enhanced confinement via positive feedback between $|\beta'|$ and microstability. In tokamaks, this effect might play a role in internal transport barriers (ITBs) with locally very steep pressure profiles. Unlike $\mathbf{E} \times \mathbf{B}$ shear stabilization, the β' stabilization mechanism has the advantages of being independent of the need for external momentum injection and of ρ^* effects. Therefore, β' stabilization may be particularly relevant for reactor scales.

II. MICROSTABILITY ANALYSIS CODE BENCHMARKING AT HIGH β

The tool used for the microstability analysis is a linear gyrokinetic electromagnetic flux tube code, GS2 (Ref. 1). The gyroaveraged Vlasov equation, coupled to the Maxwell equations, is solved. The growth rates of the unstable modes are computed. The electrons and ions, passing and trapped, respond to the perturbed fields: $\delta\phi$, δB_{\parallel} , and δB_{\perp} . This

^{a)}Electronic mail: clarisse.bourdelle@cea.fr

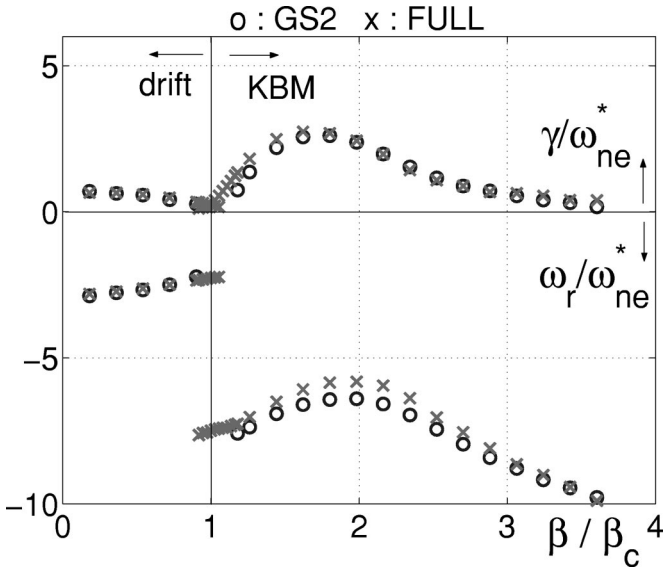


FIG. 1. Results from the initial value and eigenvalue calculations: the growth rates γ and the frequencies ω_r in units of ω_{ne}^* vs the local total β normalized to a β_c of 2%. β is proportional to the MHD equilibrium parameter α . Fixed $k_{\theta}\rho_i=0.4$.

implies that ion temperature gradient modes (ITG), trapped electron modes (TEM), as well as electron temperature gradient modes (ETG) are included. The magnetic modes known as kinetic ballooning modes (KBM, also called Alfvén ion temperature gradient modes, AITG) are also accessible, as well as microtearing modes. In gyroaveraging the Vlasov equation, it is assumed that the Larmor radii and the banana widths (symbolized by ρ) are much smaller than the characteristic lengths of the plasma, such as the gradient length (symbolized by L_P). The main limitation to flux tube codes is that they use the ballooning representation, which is valid at wavelengths (λ) much smaller than any gradient length characteristic of the studied plasma. Therefore,

$$\begin{aligned} \rho &\ll L_P, \\ \lambda &\ll L_P. \end{aligned} \quad (1)$$

Two of the existing linear gyrokinetic electromagnetic flux tube codes are benchmarked for high values of β which are relevant for NSTX plasmas. Good agreement is found with these codes, each of which uses a different computational method. FULL (Refs. 3 and 4) implements an eigenvalue calculation, whereas GS2 (Ref. 1) uses an initial value approach to find the fastest growing mode. A previous benchmark of these two codes has been published in Ref. 1. Figure 5 of Ref. 1 shows good agreement between the two codes for β values up to 2%, including the effects of $\delta\phi$ and δB_{\perp} only. In Fig. 1, the benchmarking exercise is extended to include δB_{\parallel} and values of β over 2%. The plasma is an L-mode discharge from the Tokamak Fusion Test Reactor (TFTR), shot 49982, at $r=38$ cm. An “ $s-\alpha$ ” model MHD equilibrium is used. Together with the main ions and the electrons, a carbon impurity species is included and a hot deuterium species representing the neutral beam fast ions is also included. Electron collisions are included, but ions collisions are neglected. The complete set of parameters used can be

found in Ref. 1. For reference here, $R/L_{ne} = - (R/n_e) \times (\partial n_e / \partial r) = 1.48$, $\eta_e = 4.683$, $q = 2.2515$, and $s = 1.1025$. For β around its critical value β_c , the drift branch becomes stable and the kinetic ballooning modes (see, for example, Refs. 4, 6, 9, 10) are destabilized by interchange with an Alfvénic wave at sufficiently large pressure gradient. The kinetic β_c found here is inferred to be lower than the ideal MHD β_c as already observed with FULL in Ref. 4 and also in Ref. 9. For the drift branch, good agreement between the two calculations is found, with $|\Delta\omega|/|\omega| \leq 6\%$. On the KBM branch, the agreement is also good with $|\Delta\omega|/|\omega| \leq 15\%$ (Fig. 1).

III. IMPACT OF β' ON DRIFT MODES

The magnitude and direction of the curvature and ∇B drifts are of prime importance. If they follow the direction of the diamagnetic drift they are responsible for the dominant interchange instability. On the other hand, if their direction is opposite to the diamagnetic drift no interchange type instability appears no matter how steep the density and temperature profiles. For a simple picture of curvature-driven instabilities, see Ref. 11. Low or negative magnetic shear is known to reduce significantly the amplitude of the curvature and ∇B drifts. In the following we will show that high $|\beta'|$ also does so. The stabilizing $|\beta'|$ effect is particularly interesting since it is enhanced by steeper pressure profile, allowing for positive feedback between steep plasma pressure and turbulence suppression.

In the ballooning or field-line following limit, we assume that the perturbed quantities A vary as

$$A = \hat{A}(\theta) \exp(in\sigma), \quad (2)$$

where $\hat{b} \cdot \nabla\sigma = 0$ and $\sigma = (\varphi - q(\psi)\theta)$, with φ and θ , respectively, the toroidal and poloidal angles (using a coordinate system in which field lines are straight), and q the safety factor. The exponential factor $\exp(in\sigma)$ represents the rapid cross-field variation with a perpendicular wave vector $\mathbf{k}_{\perp} \equiv n\nabla\sigma$. The factor $\hat{A}(\theta)$ gives the slow variation of the mode along the field line. An important parameter affecting stability is the drift frequency $\omega_d = \mathbf{v}_d \cdot \mathbf{k}_{\perp}$, which is

$$\omega_d = \frac{V_{\parallel}^2}{\omega_c} n\omega_{\kappa} + \frac{\mu B}{m\omega_c} n\omega_{\nabla B}, \quad (3)$$

where the normalized curvature and ∇B drifts are $\omega_{\kappa} = \hat{b} \times (\hat{b} \cdot \nabla\hat{b}) \cdot \nabla\sigma$ and $\omega_{\nabla B} = (\hat{b} \times \nabla B \cdot \nabla\sigma)/B$. Here, ω_c is the cyclotron frequency. \hat{b} is the direction of the magnetic field line and B is the magnetic field strength.

The so-called $s-\alpha$ analytical equilibrium is valid at high β and high aspect ratio for circular concentric magnetic surfaces; s is the magnetic shear and $\alpha = -q^2 R\beta' = -q^2 R\beta(\partial P/\partial r)/P$. In this case the normalized ∇B and curvature drifts are proportional to

$$\begin{aligned} \omega_{\kappa} &\propto \cos\theta + (s\theta - \alpha \sin\theta)\sin\theta, \\ \omega_{\nabla B} &\propto \cos\theta + (s\theta - \alpha \sin\theta)\sin\theta - \frac{\alpha}{2q^2}. \end{aligned} \quad (4)$$

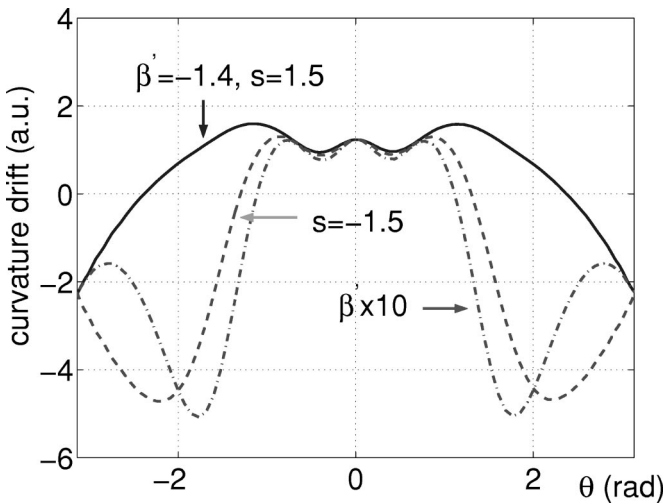


FIG. 2. Curvature drift vs the poloidal angle θ . The effects of multiplying $\beta' \times 10$ and $s \times (-1)$ are compared.

In this simplified geometry, a high value of $|\beta'|$ (i.e., high α) lowers the surface average of the curvature and ∇B drifts, and therefore lowers the destabilizing impact of the interchange instability. From the similar ways in which α and s enter this equation, one can see that the stabilizing effect of high α can be thought of as being similar to a local negative shear. A nice physical picture of the stabilizing influence of negative magnetic shear is in Ref. 16. Note that α has also an effect on $\omega_{\nabla B}$ in the center of the bad-curvature region at $\theta = 0$. This effect is referred as the “self-dug” magnetic well.

A more general form of Eq. (4) using the equilibrium relation $\nabla p = \mathbf{j} \times \mathbf{B}$ and vector identities gives

$$\omega_{\nabla B} = \omega_{\kappa} - \frac{1}{2} \hat{\mathbf{b}} \times \nabla \beta \cdot \nabla \sigma, \quad (5)$$

where we are using the shorthand notation $\nabla \beta \equiv (2\mu_0/B^2) \nabla p$. Therefore the total drift frequency becomes

$$\omega_d = \left(\frac{V_{\parallel}^2}{\omega_c} + \frac{\mu B}{m\omega_c} \right) n\omega_{\kappa} - \frac{\mu B n}{m\omega_c} \frac{\beta}{2} \frac{\hat{\mathbf{b}} \times \nabla p}{p} \cdot \nabla \sigma. \quad (6)$$

Using a numerical NSTX magnetic equilibrium computed by EFIT (Ref. 12), one may vary $|\beta'|$ and the magnetic shear s independently to find a family of solutions, all of which satisfy the Grad–Shafranov equation (see, for example, Refs. 13 and 14). In Figs. 2 and 3, the impact of magnetic shear reversal on the curvature and ∇B drifts is compared to the impact of higher $|\beta'|$. The ∇B drift is especially strongly decreased by high $|\beta'|$ (Fig. 3). When the curvature and ∇B drifts are positive, they are able to destabilize the interchange. When they are negative, their direction is opposite to the diamagnetic direction and no interchange destabilization is possible. One can note that, in Figs. 2 and 3, the difference $\omega_{\kappa} - \omega_{\nabla B}$, obtained with an NSTX computed equilibrium, is dependent of poloidal angle, whereas the simplified “ $s-\alpha$ ” model gives $\omega_{\kappa} - \omega_{\nabla B} = \alpha/2q^2$, which is independent of θ . This emphasizes that for a low aspect ratio machine a computed magnetic equilibrium is necessary to produce accurate results.

The stabilizing effect of high $|\beta'|$ on the ∇B drift is known as the effect of the “self-dug” magnetic well. At long

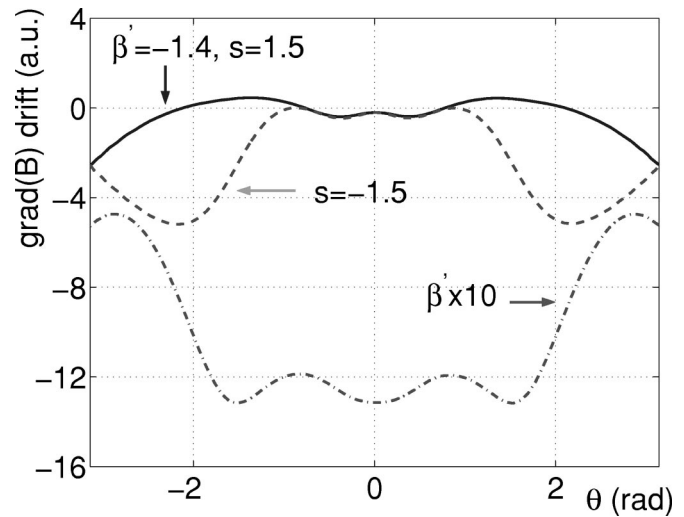


FIG. 3. ∇B drift vs the poloidal angle θ . $\theta=0$ is on the low field side. The effects of multiplying $\beta' \times 10$ and $s \times (-1)$ are compared.

wavelengths ($k_{\perp} \rho_i \ll 1$) and low frequencies ($\omega \ll \Omega_{ci}$) this effect is of limited importance, as detailed in Ref. 15. This is because compressional motion acts to maintain perpendicular force balance $\delta p_{\perp} + B_0 \delta B_{\parallel} / \mu_0 = 0$, with the consequence that there is a significant cancellation between the diamagnetic drift and the part of the grad-B drift proportionnal to ∇P in the vorticity equation [see Ref. 7, Eq. (63) for details]. Therefore, if one does not include δB_{\parallel} at high β , the self-dug well stabilizing impact is artificially overestimated. Hence, it is of prime importance to include δB_{\parallel} for high β microstability analysis. Nevertheless, for finite $k_{\perp} \rho_i$, some stabilization from the self-dug well remains possible, as seen in Refs. 6, 15, 8. Even in cases where the self-dug well effects are mostly cancelled, high $|\beta'|$ still has a stabilizing effect on the curvature drift (as seen in Fig. 2) via the negative local magnetic shear (Ref. 16) it induces.

In Figs. 4 and 5, a scan of β' at fixed β and at fixed η is shown for a case with ion modes only ($\nabla T_e / T_e = 0$ and

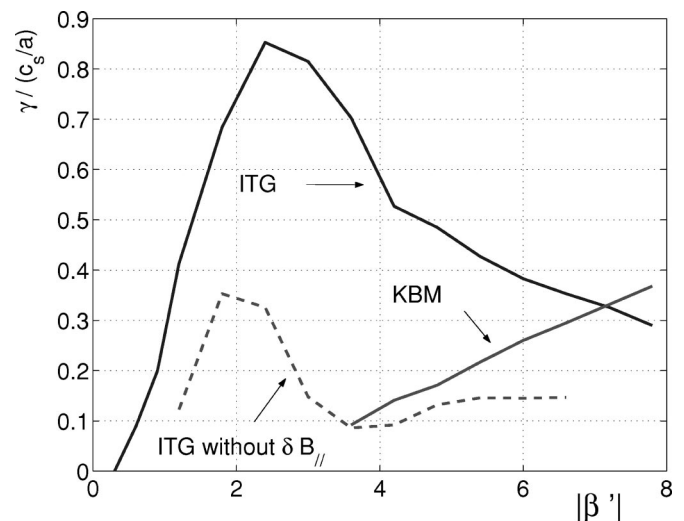


FIG. 4. Growth rates vs $-\beta'$ using a numerical MHD equilibrium, at $\beta = 30\%$, $s = 1.3$, $\nabla T_e / T_e = 0$, $\nabla n_e / n_e = 0$, and $\eta_i = 3$. For ITG modes $k_{\theta} \rho_i \approx 0.4$, for KBM $k_{\theta} \rho_i \approx 0.15$. Full line: with $\delta \phi$, δB_{\perp} , and δB_{\parallel} ; dashed line: with $\delta \phi$ and δB_{\perp} only.

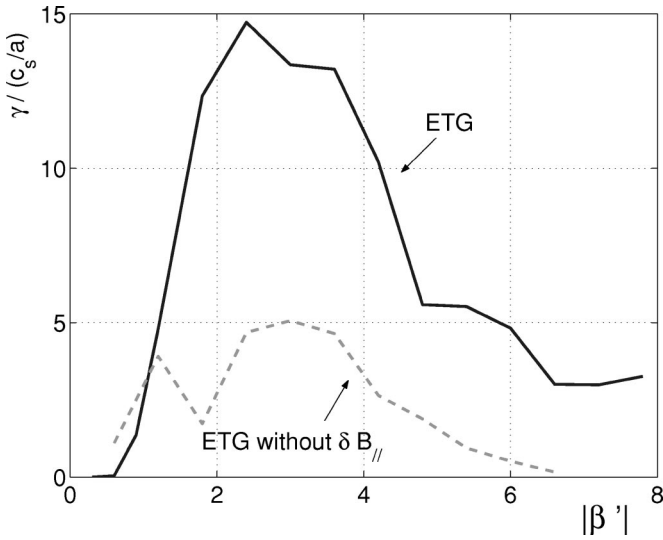


FIG. 5. Growth rates vs $-\beta'$ using a numerical MHD equilibrium, at $\beta = 30\%$, $s = 1.3$, $\nabla T_i/T_i = 0$, $\nabla n_i/n_i = 0$, and $\eta_e = 3$. $k_{\theta}\rho_e \approx 0.3$. Full line: with $\delta\phi$, δB_{\perp} , and δB_{\parallel} ; dashed line: with $\delta\phi$ and δB_{\perp} only.

$\nabla n_e/n_e = 0$) and for another case with electron modes only ($\nabla T_i/T_i = 0$ and $\nabla n_i/n_i = 0$). The equilibrium used is computed by TRANSP for the NSTX discharge 106382 at 210 ms. At $r/a = 0.34$ where the local total β is 30%. The magnetic shear is fixed at 1.3. In this exercise, it is increased by increasing the local pressure gradient $|\nabla P/P|$, keeping all of the other equilibrium parameters fixed while still satisfying the Grad-Shafranov equation (see Ref. 14) solved by TRANSP numerical equilibrium. The equilibrium is therefore not globally recalculated but only locally changed while scanning $|\beta'|$. In these scans, $\beta' = \beta(a/L_n)(1 + \eta)$ and $\eta = n\partial T/\partial r/T\partial n/\partial r = L_n/L_T$ is kept fixed and equal to 3. Despite the steeper pressure profiles, the drift modes (ITG, TEM, and ETG) are ultimately stabilized by higher $|\beta'|$. This indicates that steep pressure profiles can be stabilizing, causing steeper pressure profiles. However, the KBM remain unstable at high $|\beta'|$ and thus may limit the achievable $|\beta'|$.

As expected, the comparison between the β' scans in Figs. 4 and 5 with and without δB_{\parallel} shows that neglecting δB_{\parallel} in high β plasmas leads to a clear underestimation of the growth rates as well as an overestimation of the stabilizing β' impact.

The magnetic shear is then reduced from 1.3 to 0.3; 0.3 being actually the value given by the EFIT equilibrium at the chosen radius. The same β' scan at fixed η is performed. In Fig. 6, the 2 scans for $s = 1.3$ and $s = 0.3$ are compared. One can see that the 2 stabilizing effects of low magnetic shear and high $|\beta'|$ combine, making it either for high values of $|\beta'|$ to be stabilizing.

In summary of this section, the mechanism leading to microturbulence stabilization through high $|\beta'|$ is similar to the impact of magnetic shear reversal. However, unlike the case of magnetic shear, β' is reinforced by steeper pressure profiles, opening the door to positive feedback between steep plasma pressure and good confinement. This is similar to the situation with increased rotational shear stabilization by increased pressure gradients. We have also shown that neglect-

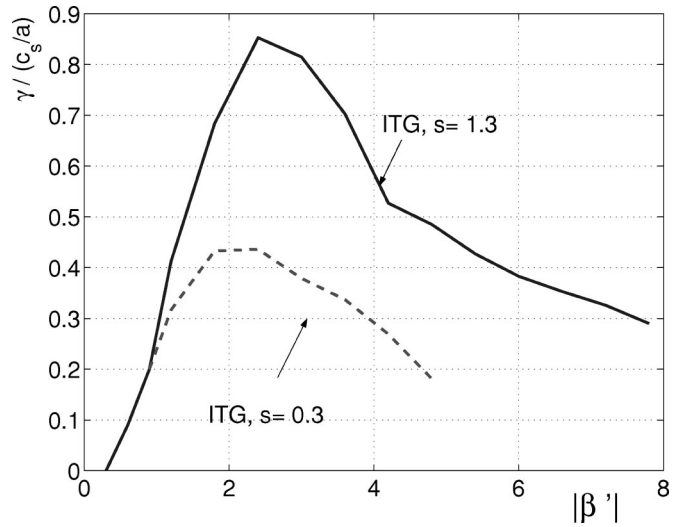


FIG. 6. Growth rates vs $|\beta'|$ as for Fig. 4. Full line: $s = 1.3$; dashed line: $s = 0.3$.

ing δB_{\parallel} when analyzing high β plasmas leads to an underestimation of the growth rates.

IV. β' IMPACT ON THE MICROSTABILITY OF A SPHERICAL TOKAMAK

The main differences between spherical tokamak (ST) and standard tokamak equilibria are the aspect ratio (A), β and β' . The NSTX aspect ratio is 1.3 compared to DIII-D's aspect ratio of 2.7. The highest volume average toroidal β obtained in NSTX is about 34%, whereas in standard tokamaks it is typically below 3%, but can occasionally reach up to 11% as it has been the case in DIII-D (Ref. 17). Since we want to elucidate the separate impact of β and A as well as β' , we cannot use a realistic numerical MHD equilibrium verifying the Grad-Shafranov equation. We therefore use an analytical equilibrium. The tokamak case and the ST case match realistic equilibrium values from DIII-D and NSTX EFIT equilibria at midradius. But the intermediate cases where A , β , and β' are varied one by one do not match realistic equilibria. The Miller model is used for the poloidal crosssection of the magnetic surface (Ref. 5). Collisions are not included here. The parameters for the Miller model are:

$$r/a = 0.5, \Delta' = (\partial\Delta/\partial\rho)/a = -0.25,$$

$$s = 1.5, \quad q = 1.5,$$

$$\kappa = 1.5, \quad \kappa' = \partial\kappa/\partial\rho = 0.25,$$

$$\delta = 0.1, \quad \delta' = \partial\delta/\partial\rho = 0.08,$$

$$T_e = T_i = 1.5 \text{ keV}, \quad n_e = n_i = 2.10^{19} \text{ m}^{-3},$$

$$\frac{1}{T} \left| \frac{\partial T}{\partial \rho} \right| = a/L_T = 4, \quad \frac{1}{n} \left| \frac{\partial n}{\partial \rho} \right| = a/L_n = 2, \quad (7)$$

ρ is the normalized square root of the toroidal flux, Δ is the Shafranov shift normalized to the minor radius, κ is the elongation, and δ is the triangularity. Note that the density and temperature values given here are more relevant for NSTX

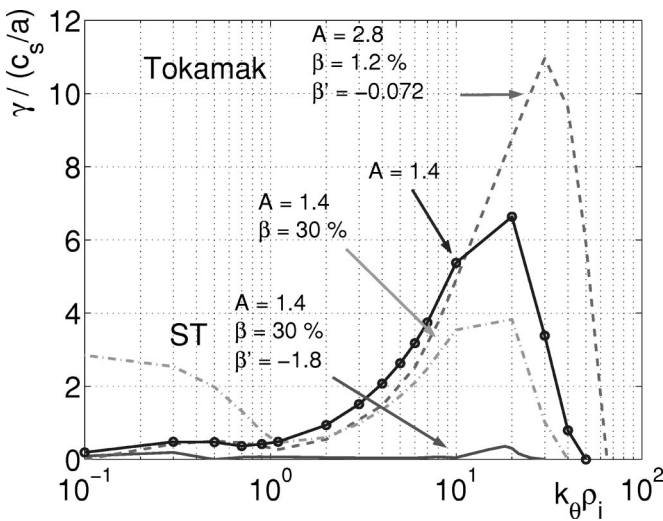


FIG. 7. Spectrum of normalized growth rates. a is the minor radius, $c_s = \sqrt{T/m_D}$, $\rho_s = \sqrt{Tm_D}/(eB)$. Dashed line: $A=2.8$, $\beta=1.2\%$, $\beta'=-0.072$; solid line with dots: $A=1.4$, $\beta=1.2\%$, $\beta'=-0.072$; dashed and dotted line: $A=1.4$, $\beta=30\%$, $\beta'=-0.072$; solid line: $A=1.4$, $\beta=30\%$, $\beta'=-1.8$.

midradius plasmas, but will nevertheless be used for the DIII-D like case in order to isolate the key parameters A , β , and β' .

For the DIII-D like case, $A=2.8$, $\beta=1.2\%$ ($B=2$ T), and $\beta'=-0.072$. For the NSTX-like case, $A=1.4$, $\beta=30\%$ ($B=0.4$ T), and $\beta'=-1.8$. It is interesting to note that the radial gradient of the Shafranov shift (Δ') is similar for both equilibria. For a low β , high A equilibrium, $(\Delta')_{r=a} = -(a/R)(\beta_p + (li/2))$. This formula is not accurate for an ST plasma. Nevertheless, the fact that Δ' is not higher in an ST is likely due to similar poloidal magnetic field values in an ST and in a tokamak. In NSTX, the plasma current ranges from 0.5 to 1.5 MA, similar to tokamak values, whereas the toroidal magnetic field ranges between 0.3 to 0.45 T, below tokamak values. Therefore, a higher $|\Delta'|$ is not a clear source of stabilization in an ST despite what was proposed in the conclusion of Ref. 18. The main results in Ref. 18 used a full numerical equilibrium including both Δ' and β' stabilization effects. Unlike here, the scans were done globally by changing the density profile, therefore changing Δ' and β' simultaneously.

We go from the DIII-D like case to the NSTX like case by changing first A only, then A and β , and finally A , β , and β' , as shown in Figs. 7 and 8. Since $\beta' = -\beta(a/L_T + a/L_n)$, rigorously it may seem inconsistent to vary these separately. But these parameters enter the gyrokinetic equations in various ways representing different physics, so it is useful to vary them one at a time. β' enters the equilibrium and thus ω_d as described earlier. β enters Ampère's law and thus affects the relative magnitude of magnetic and electric fluctuations, while a/L_n and a/L_T appear in the definitions of the diamagnetic drifts.

We observe that lowering the aspect ratio stabilizes the modes above $k_\theta \rho_i = 10$, the ETG modes. This is due to the effect of passing particles spending more time on the good curvature side at low aspect ratio, as already pointed out in

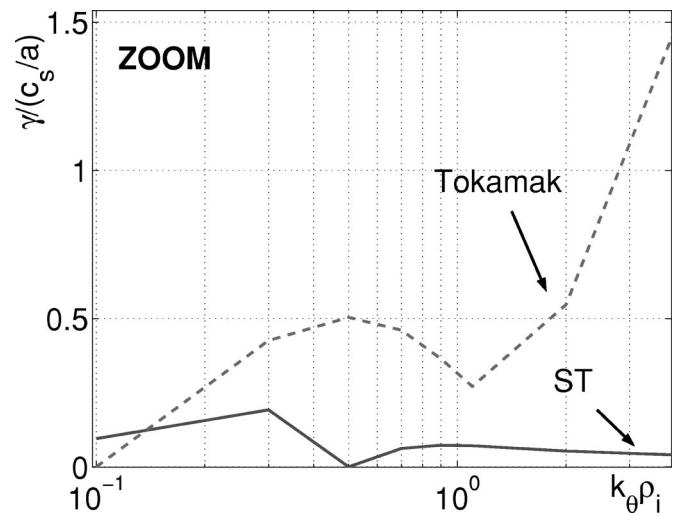


FIG. 8. Enlargement of Fig. 7 in the low $k_\theta \rho_i$ zone for the tokamak-like case, dashed line, and the ST-like case, solid line.

the case of passing ions in Ref. 19. The modes between $k_\theta \rho_i = 1$ and $k_\theta \rho_i = 10$ are slightly destabilized by a lower aspect ratio. These modes are dominated by trapped electrons (TEM). At low aspect ratio, the depth of the magnetic well is larger since $\Delta B_T/B_{T0} \approx 2A/(A^2-1)$. Therefore the fraction of trapped particles is higher. Finally modes below $k_\theta \rho_i = 1$ are almost unaffected; in this range trapped and passing ions are expected to be the dominating resonating particles. In this case, the stabilizing effect through passing particles and the destabilizing effect through trapped particles annihilate each other when going to lower A . When β is also increased from 1.2% to 30%, kinetic ballooning modes are destabilized at low k_θ whereas the upper part of the spectrum is stabilized. In Ref. 8, it is shown that when KBM are not destabilized, ITG modes are not affected by a lower A , if β remains at a fixed fraction of the ideal MHD β limit, which is higher in an ST than in a standard tokamak. Finally, when $|\beta'|$ is increased, all the modes are clearly strongly stabilized. Therefore, the main mechanism responsible for the more stable modes obtained with an ST-like set of equilibrium parameters is due to a higher value of $|\beta'|$. This very strong impact of $|\beta'|$ is confirmed by running the tokamak-like case changing only β' from -0.072 to -1.8 . Indeed in the ITG range, the growth rates are as low as half of the ST like case, and the ETG are completely stabilized. As detailed in Sec. III, the stabilizing impact of high $|\beta'|$ is due to lower drive from curvature and ∇B drifts for the inter-change instability.

V. POSSIBLE EXPERIMENTAL TEST OF β' IMPACT IN NSTX

The fact that the plasma becomes more stable with higher $|\beta'|$ opens a wider window towards positive feedback between a steep pressure profile and good confinement.

In Figs. 9 and 10, the normalized temperature gradient (a/L_T) is increased consistently with β' . β is fixed and η varies, unlike in Figs. 4 and 5 which were obtained at fixed η . Note here that the effect of collisions is not included. A

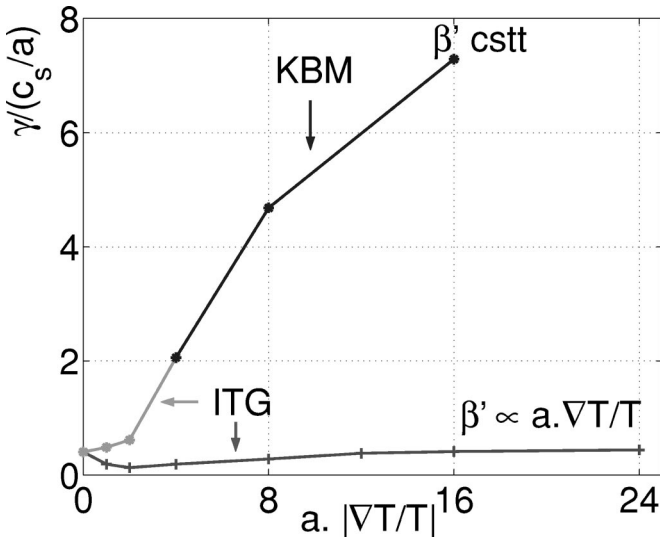


FIG. 9. Normalized maximum growth rates for $k_{\theta}\rho_i < 1$ as a function of normalized temperature gradient. Solid line and crosses: the temperature gradient is increased consistently with β' . Solid line and dots: the temperature gradient is increased with β' fixed at the value it had for $a/L_T=0$.

steeper temperature profile is likely to be accompanied by a higher temperature, and therefore a lower collisionality that might enhance the role of trapped particles. Nevertheless, the collisions being stabilizing, we are presenting here an upper limit of the growth rates. In Fig. 9, the consistent temperature gradient scan is compared with a scan where β' is artificially kept fixed. In the latter case, the growth rates reach much higher values when a/L_T is increased. In particular, the KBM are destabilized. Therefore, β' stabilization allows us to avoid triggering KBM. Figure 10 shows that the growth rates in an ST plasma increase less with higher temperature gradients and higher η than for a tokamak case. This happens thanks to higher β , and therefore higher $|\beta'|$, in the ST case. In the ST case, the growth rates increase at low values of

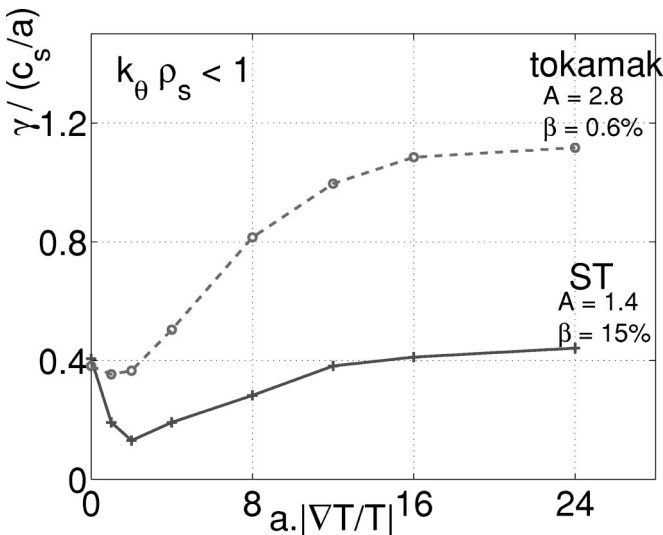


FIG. 10. Normalized maximum growth rates for $k_{\theta}\rho_i < 1$ as a function of normalized temperature gradient. The temperature gradient is increased consistently with β' . Solid line and crosses: for the ST-like configuration; solid line and dots: for the tokamak-like configuration as defined in Fig. 7.

a/L_T due to a more important role of trapped particles when $\eta < 1$. Since the trapped particle fraction is more important in the ST configuration, the ST growth rates become similar to the tokamak ones. Above $a/L_T=2$, the increase of the temperature gradient is destabilizing, but much less so in the ST case than in the tokamak case. Therefore, in the ST case, the stabilization of these low k_{θ} modes by the $\mathbf{E} \times \mathbf{B}$ shear is made easier by lower growth rates. At fixed η , in Figs. 4 and 5, it is shown that positive feedback on the confinement due to $|\beta'|$ alone can be reached for sufficiently high $|\beta'|$. Very likely a combination of density peaking and $|\beta'|$ stabilization would even be more efficient. And as we have shown in Fig. 6, a combination of magnetic shear reversal and high $|\beta'|$ is expected to make easier the $|\beta'|$ stabilization. This possibility of positive feedback is very similar to the one proposed by Beer in Ref. 18 to explain the enhanced reversed shear modes obtained in TFTR, except that the stabilizing mechanism triggering the improvement was due to higher Δ' , whereas here it is due to higher $|\beta'|$.

To test experimentally the β' impact on microturbulence one would ideally need a set of plasmas where T_i/T_e , Z_{eff} , s , q , ρ^* , β , as well as the $\mathbf{E} \times \mathbf{B}$ shearing rate, are kept fixed while $|\beta'|$ (i.e., $|\nabla P|/P$) is increased. More generally, the clearest demonstration of the role of β' would arise if the $\mathbf{E} \times \mathbf{B}$ shear and β' could be decoupled. These constraints are practically impossible to realize in a β' scan. Nevertheless, there are some ways to approach such a scan: by using pellet injection in order to peak the density, by applying some early heating in the current ramp-up phase to increase the Shafranov shift and therefore the pressure gradient or by performing a power scan of balanced NBI at fixed B_T and I_p . The β' stabilization might be used to trigger an improved confinement regime on its own, but more likely by lowering the growth rates with respect to the $\mathbf{E} \times \mathbf{B}$ shearing rate. Indeed, similarly, RI modes and certain ITB regimes are believed to be triggered by, respectively, higher Z_{eff} and magnetic shear reversal and then maintained by $\mathbf{E} \times \mathbf{B}$ shear (see, for example, Ref. 20).

VI. CONCLUSIONS

The behavior of microinstabilities with β' has been investigated with a gyrokinetic electromagnetic flux tube code, GS2. It is found that the stability of all types of drift modes (ITG, TEM, ETG) is strongly increased by high values of $|\beta'|$. It is shown that high $|\beta'|$ reduces the drive of the ∇B and curvature drifts responsible for the interchange instability. This stabilizing impact is overestimated by about a factor of 2 in high β plasmas if the magnetic perturbations parallel to the field (δB_{\parallel}) are neglected. In high β experimental spherical tokamak plasmas, it is shown that β' has more impact than low aspect ratio itself on the linear microstability. Experimental tests of this impact are needed, by either fruitfully exploiting the easier $\mathbf{E} \times \mathbf{B}$ shear stabilization due to lower growth rates, or by reaching a $|\beta'|$ high enough to lead to positive feedback without the help of $\mathbf{E} \times \mathbf{B}$ shear, but likely with the help of magnetic shear reversal or density

peaking. Initial results from NSTX (Ref. 21) indicate that thermal ion confinement is exceptionally good, and the role of β' is being assessed.

The stabilizing impact of high $|\beta'|$ might also be relevant in low β tokamak plasmas when a locally steep pressure gradient is maintained without external momentum injection (see, for example, Refs. 22 and 23).

ACKNOWLEDGMENTS

We thank the NSTX team and Doug McCune, for their help.

This work was supported by the U.S. Department of Energy Contract No. DE-AC02-76CH03073.

- ¹M. Kotschenreuther, G. Rewoldt, and W. M. Tang, *Comput. Phys. Commun.* **88**, 128 (1995).
²M. Kotschenreuther, W. Dorland, Q. P. Liu *et al.*, in Proceedings, 16th IAEA Fusion Energy Conference, Montreal, 1996, paper CN-64, D1-5.
³G. Rewoldt, W. M. Tang, and M. S. Chance, *Phys. Fluids* **25**, 480 (1982).
⁴G. Rewoldt, W. M. Tang, and R. J. Hastie, *Phys. Fluids* **30**, 807 (1987).
⁵R. L. Miller, M. S. Chu, J. M. Greene, Y. R. Lin-Liu, and R. E. Waltz, *Phys. Plasmas* **5**, 973 (1998).
⁶W. M. Tang, J. W. Connor, and R. J. Hastie, *Nucl. Fusion* **20**, 1439 (1980).

- ⁷A. Brizard, *Phys. Fluids B* **4**, 1213 (1992).
⁸M. Kotschenreuther, W. Dorland, Q. P. Liu, M. C. Zarnstorff, R. L. Miller, and Y. R. Lin-Liu, *Nucl. Fusion* **40**, 677 (2000).
⁹G. Zhao and L. Chen, *Phys. Plasmas* **9**, 861 (2001).
¹⁰C. Z. Cheng, *Phys. Fluids* **25**, 1020 (1982).
¹¹F. Jenko and W. Dorland, *Plasma Phys. Controlled Fusion* **43**, A141 (2001).
¹²S. A. Sabbagh, S. M. Kaye, J. Menard *et al.*, *Nucl. Fusion* **21**, 453 (1981).
¹³J. M. Greene and M. S. Chance, *Nucl. Fusion* **41**, 1601 (2001).
¹⁴C. M. Bishop, P. Kirby, J. W. Connor, R. J. Hastie, and J. B. Taylor, *Nucl. Fusion* **24**, 1579 (1984).
¹⁵H. L. Berk and R. R. Dominguez, *J. Plasma Phys.* **18**, 31 (1977).
¹⁶T. M. Antonsen, Jr., J. F. Drake, P. N. Guzdar, A. B. Hassam, Y. T. Lau, C. S. Liu, and S. V. Novakovskii, *Phys. Plasmas* **3**, 2221 (1996).
¹⁷E. A. Lazarus, L. L. Lao, T. H. Osborne, and T. S. Taylor, *Phys. Fluids B* **4**, 3644 (1992).
¹⁸M. A. Beer, G. W. Hammett, G. Rewoldt, E. J. Synakowski, M. C. Zarnstorff, and W. Dorland, *Phys. Plasmas* **4**, 1792 (1997).
¹⁹G. Rewoldt, W. M. Tang, S. Kaye, and J. Menard, *Phys. Plasmas* **3**, 1667 (1996).
²⁰C. Bourdelle, X. Garbet, G. T. Hoang, J. Ongena, and R. V. Budny, *Nucl. Fusion* **42**, 892 (2002).
²¹E. J. Synakowski, M. G. Bell, R. E. Bell *et al.*, *Plasma Phys. Controlled Fusion* **44**, A165 (2002).
²²G. T. Hoang, C. Bourdelle, X. Garbet *et al.*, *Phys. Rev. Lett.* **84**, 4593 (2000).
²³J. E. Rice, P. T. Bonoli, E. S. Marmor *et al.*, *Nucl. Fusion* **42**, 510 (2002).